

Preliminary Characterization of a NAPL-Contaminated Site using Borehole Geophysical Techniques

[Jonathan B. Ajo-Franklin](#) Stanford University, Stanford, CA.

[Jil T. Geller](#) Lawrence Berkeley National Laboratory, Berkeley, CA.

[Ernest L. Majer](#) Lawrence Berkeley National Laboratory, Berkeley, CA.

[John E. Peterson](#) Lawrence Berkeley National Laboratory, Berkeley, CA.

[Kenneth H. Williams](#) Lawrence Berkeley National Laboratory, Berkeley, CA.

[Jerry M. Harris](#) Stanford University, Stanford, CA.

Abstract

We present preliminary results from an on-going geophysical investigation of the former DOE Pinellas site, a site with confirmed non-aqueous phase liquid (NAPL) contamination. Our eventual goal is the effective use of integrated crosswell geophysical methods, specifically seismic and radar tomography, to remotely detect zones of high NAPL saturation. In this paper we discuss our motivation and early efforts at using a combination of seismic and radar information to understand site geology and possible contaminant signatures. We also present our current approach to consistent acquisition, preprocessing, tomographic inversion, and interpretation of joint seismic/radar profiles. Although direct geophysical evidence of NAPL pools has not yet been obtained, several regions of anomalous seismic attenuation were detected. These attenuating regions could not be explained by borehole effects or lithology and may be caused by regions of partial gas or NAPL saturation. Possible gas sources include biogenic production from contaminated regions and side-effects from previous remediation activities. Continuing research at the Pinellas site will focus on constraining the mechanism responsible for the observed seismic attenuation, developing a more complete model of site soil properties, and applying more quantitative approaches to the integration and analysis of our seismic and radar images.

1 Introduction: The Pinellas Project

The detection and delineation of non-aqueous phase liquids (NAPLs) using geophysical methods is a challenging problem which has been considered, with varying degrees of success, for both controlled release scenarios [7] [6] [29] [27] and previously existing contaminant sites [31] [13]. An outstanding problem with previous field studies is the difficulty in distinguishing the geophysical signatures of NAPLs from existing lithological variations which cause similar changes in physically observable properties, such as dielectric constant. This problem is particularly striking when only surface GPR data is available for imaging purposes.

Driven by recent core scale and physical modeling studies of the acoustic properties of NAPLs [11] [30] [16] [10], we have embarked on a pilot project to geophysically detect NAPLs using a combination of crosswell radar and seismic methods with further constraining information derived from cone penetrometry and natural gamma measurements. This paper presents preliminary results from our on-going geophysical investigation of a former U.S. Department of Energy (DOE) facility in Pinellas County, Florida, a site with confirmed NAPL contamination. In addition to detailing the site, acquisition strategy, and processing approach we will consider the general problem of integrating seismic and radar tomograms for environmental characterization purposes. Two regions of the site, one within the zone of known NAPL contamination (the “dirty” zone) and one outside the suspected NAPL zone but still within the dissolved contaminant plume (the “clean” zone) will be examined in detail.

Although direct geophysical evidence of NAPL pools has not yet been obtained, several regions of anomalous seismic attenuation were detected. These attenuating regions could not be easily explained by borehole effects or lithology and may be caused by regions of partial gas or NAPL saturation. Possible gas sources include biogenic production from contaminated regions and side-effects from previous remediation activities.

1.1 Site History, Geology, and Existing Evidence for NAPLs

The site of our ongoing investigation is a former DOE manufacturing facility located in Pinellas County, Florida, between the cities of Clearwater and St. Petersburg. From 1956 to 1994 the [Pinellas DOE Plant](#) fabricated neutron generators, thermal batteries, vacuum switch tubes, and a variety of secondary electronic and mechanical components required for nuclear weapon construction. Over the lifetime of the facility, several chlorinated solvents were used in degreasing and cleaning capacities. Between 1957 and 1968 a small region in the Northeast section of the site, immediately west of the East Pond, was used as a drum disposal and staging area. Excavation at the Northeast Site in the latter half of 1994 revealed construction debris and drums with solvent and resin residues. The contaminants discovered in groundwater and soil sampling included trichloroethene, methylene chloride, dichloroethane, vinyl chloride, benzene, toluene, oil, and various unidentified resin compounds. Free-phase volatile organic compounds (VOCs) were also extracted from several monitoring and recovery wells, indicating the presence of a separate contaminant phase in some regions of the site. Additional evidence for NAPLs at the Northeast site was obtained during a 1996/1997 field demonstration of a [dual auger rotary steam-stripping system](#) in which high levels of VOCs overloaded the catalytic treatment system. Of the wells visible on Figure [1], free phase VOCs have been extracted from both RW03 and RW06.

The geology of our section of the NE site, as determined from a large number of visually categorized soil borings and cone penetrometry (CPT) push-points, consists of a relatively one-dimensional sequence with more subtle lateral variations. A shallow surficial aquifer consisting of fine sands and silty sands extends from the surface to a depth of approximately 10 – 11m. The surficial aquifer gradually terminates against the Hawthorn Group, an 18 – 21m thick region of silty-clays, silty-sandy clays, and carbonaceous clays. Some finer structures including zones of shell fragments, phosphate nodules, and increased silt content exist in the surficial aquifer. A definite and laterally continuous textural transition visible in all of the recorded natural gamma logs suggests

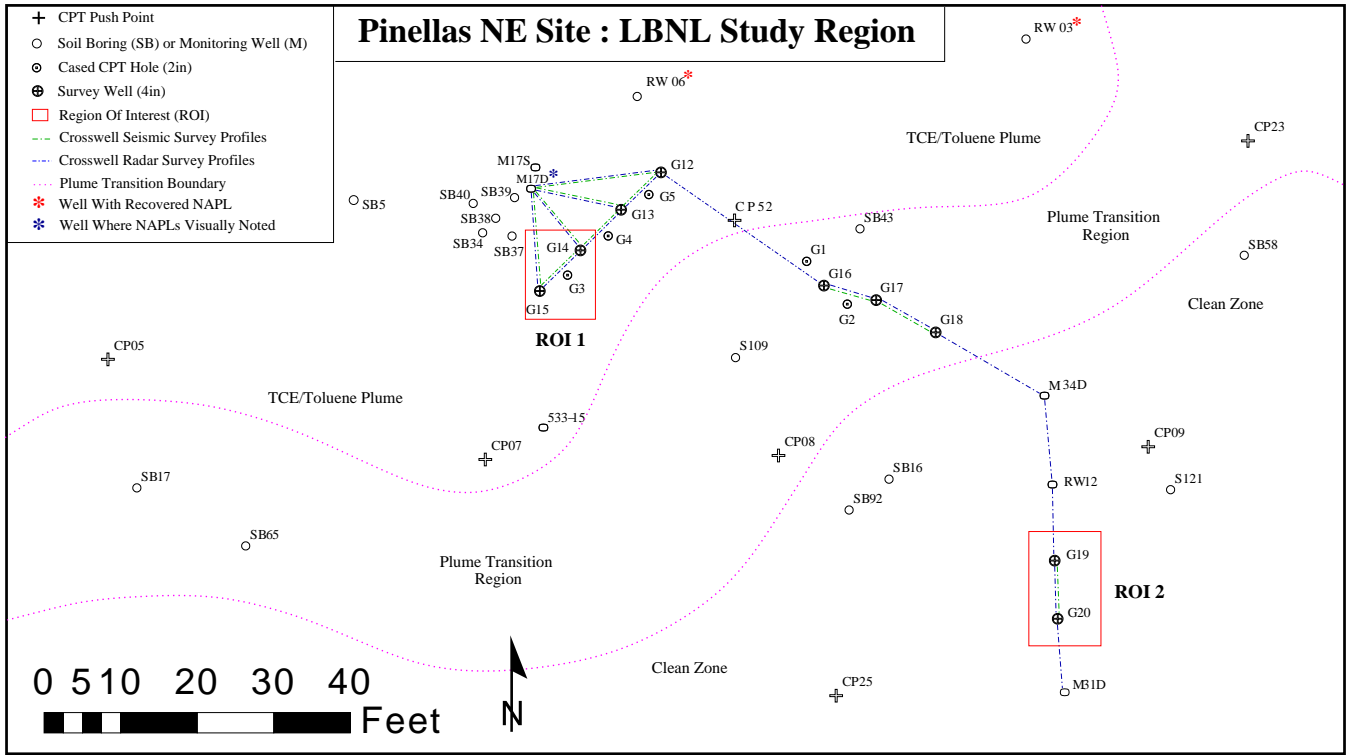


Figure 1: Pinellas NE Site Study Area

an increase in mineralogical clay content near an absolute elevation ¹ of -0.5m .

1.2 Acquired Datasets

The primary data sets acquired for our geophysical characterization of the of Pinellas NE site (see Figure [1]) consisted of a curtain of crosswell seismic profiles extending from a zone known to have NAPL contamination [ROI 1] to a region where aqueous phase contaminant levels were an order of magnitude lower but still above safe limits [ROI 2]. The crosswell seismic datasets were acquired using a 24 channel [Geometrics Geode acquisition system](#), a 24 channel hydrophone string, and a fluid coupled piezoelectric source. Nineteen seismic sections were acquired at interwell spacings ranging from 2 to 8 meters. For most crosswell seismic profiles, usable signal at up to 6.5 khz was recorded.

Crosswell radar datasets were acquired using a [Sensors & Software Pulse-Ekko 100 Borehole System](#) and 200 mhz antennas. Radar data could not be acquired in all of the wells used for seismic measurements due to the presence of conductive (steel) casing at some locations. An attempt was made to match geometries for the seismic and radar surveys by using the same source/receiver spacing (1/8 m). In addition to the crosswell measurements, a [Mount Sopris MGX II system](#) was used to acquire gamma and conductivity logs in all of the relevant wells for use in constraining lithology. Several existing CPT push-points were also available for lithology comparisons although the lack of site-specific CPT calibration data made lithology designations less certain.

¹All elevation references are made with respect to sea-level in terms of Florida State Plane coordinates. Surface elevation is approximately 6m above sea-level.

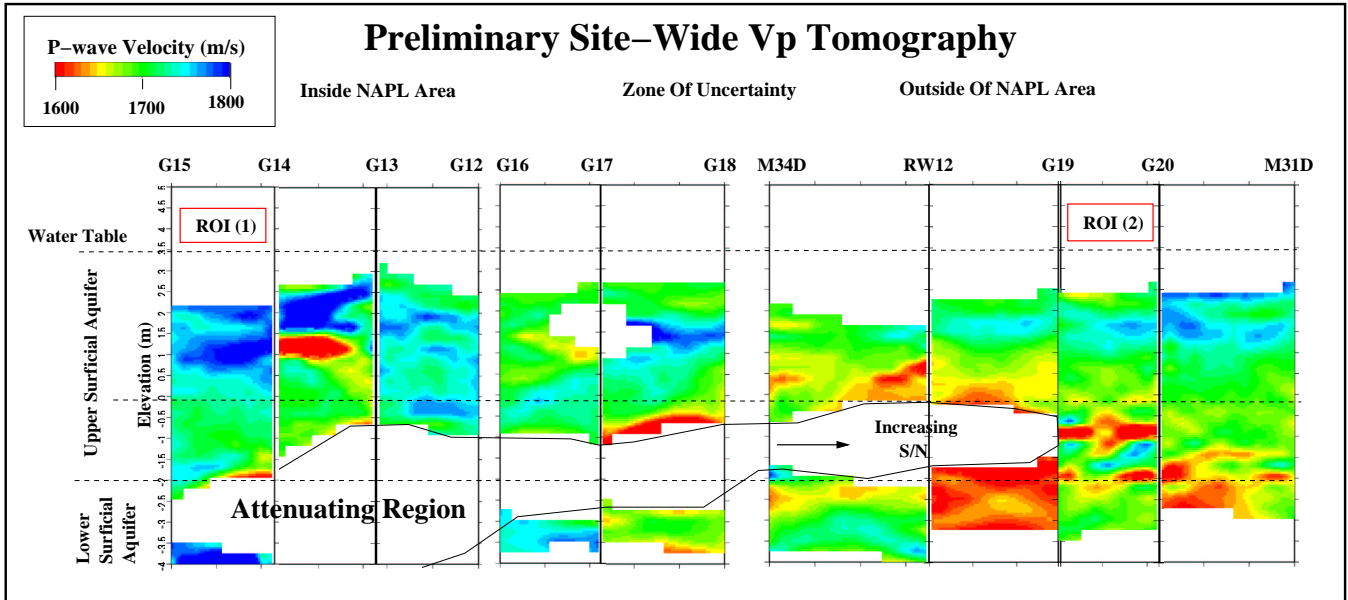


Figure 2: Preliminary Site-wide Vp Imaging Results

1.3 Preliminary Site-Wide Tomography

Two separate tomographic processing flows were applied to the crosswell data. The first flow was aimed at getting an initial set of site-wide tomographic images for immediate interpretation and the second focused on techniques for combined interpretation of the seismic and radar datasets. The initial traveltime tomography used the preprocessing steps and reconstruction techniques described in references [24] and [25] and essentially consists of 2D straight ray tomography with a damped Algebraic Reconstruction Technique (ART) solver. Although we will not describe the preliminary processing flow in detail, the referenced approach has been applied successfully to a variety of environmental imaging problems. The second tomographic flow was tailored to the combined interpretation problem and will be described in detail in the next sections.

Figure [2] depicts the preliminary site-wide P-wave velocity (V_p) section derived from nine different crosswell seismic profiles. The section stretches from well G15 (see Figure [1]), which is located within the general region of NAPL contamination, to well M31D located in a clean zone with lower aqueous phase contaminant levels. A noticeable feature is a laterally extensive zone of low signal strength which made picking difficult, when possible at all. In the preliminary processing run, pixels with insufficient ray coverage due to picking difficulties were eliminated from the inversion. The zone of high attenuation gradually decreases in expanse when moving towards the clean zone and is not visible in the last two crosswell profiles. The attenuating region is not consistent with any lithologic trends observed in well logs and may be the result of biogenic gas production associated with highly contaminated regions of the site. A more detailed discussion of the observed attenuation and various possible mechanisms is continued in Section 5.

2 Integrated Geophysics at Pinellas

The term “Integrated Geophysics” has several different meanings within the diverse community

of geoscientists. On the most basic level, integrating geophysical data is simply drawing a conclusion from multiple sets of available measurements. On the other extreme, integration refers to a complete quantitative fusion of all available data to yield a comprehensive earth model with describable resolution and error characteristics. Relatively few previous studies have attempted to integrate radar and seismic measurements and almost all have attempted integration on a purely interpretive basis after separate collection and processing of both datasets [5] [4]. Although we do not yet have a suitable strategy for a truly consistent joint inversion of our crosswell data, we have attempted to tailor our acquisition and processing flow to allow comparison and combined interpretation of the two datasets. In this section we will review the petrophysical motivation for data integration in terms of NAPL detection, an acquisition and preprocessing strategy designed to make our seismic and radar datasets comparable, our current tomographic imaging flow, and some possible routes for quantitative integration of tomography results.

2.1 A Petrophysical Motivation

One of the goals of the Pinellas project is the quantitative integration of crosswell seismic and crosswell radar data for use in characterizing subsurface fluid properties, specifically detecting regions of high NAPL saturation. NAPLs, including trichloroethene (TCE), the mostly likely NAPL in our study region, are generally non-polar with low dielectric constants (3.3 for TCE [22]) in comparison to water which has a dielectric constant of approximately 80 [1]. This property makes ground penetrating radar a good candidate technology for NAPL detection. The extensive Borden field tests [7] [6] [29] [27] convincingly demonstrated that high levels of NAPL are visible using GPR in a time-lapse sense if prior knowledge of the spill location is available. However, detection of NAPLs using dielectric properties alone seems difficult since similar radar signatures could be generated by lithological changes, including variations in matrix porosity or clay content. Recent work on the acoustic properties of NAPL saturated unconsolidated sediments [11] [30] [10] opens up the possibility of using seismic velocity or attenuation data in tandem with dielectric measurements derived from radar to more reliably predict the presence of NAPLs.

Figure [3] depicts a theoretical cross-plot of V_p and dielectric constant (κ) for a clean quartz sand subject to two property trends, one scenario where porosity is varied from 0.2 to 0.45 with a zero TCE saturation (100% water saturated, shown in red) and a second where porosity is fixed at 0.36 and TCE saturation is varied from 0 to 80% (shown in blue). The complex refractive index model (CRIM) was used to estimate effective dielectric properties. V_p was estimated by using Hertz-Mindlin contact theory [21] to determine the dry frame modulus and then saturating the pack using Gassmann's equation [9] [17] with the properties of the TCE/water mixture calculated using the Reuss effective fluid model [28] [17]. If only dielectric constant is considered, there is no reasonable way to determine whether the source of an observed radar anomaly is due to a variation in porosity or the existence of NAPLs. While we do not expect this particular combination of effective medium theories to be valid at most sites, the important insight gained from Figure [3] is the possibility of using a second data attribute, in this case V_p , to unravel lithologic trends from NAPL saturation trends.

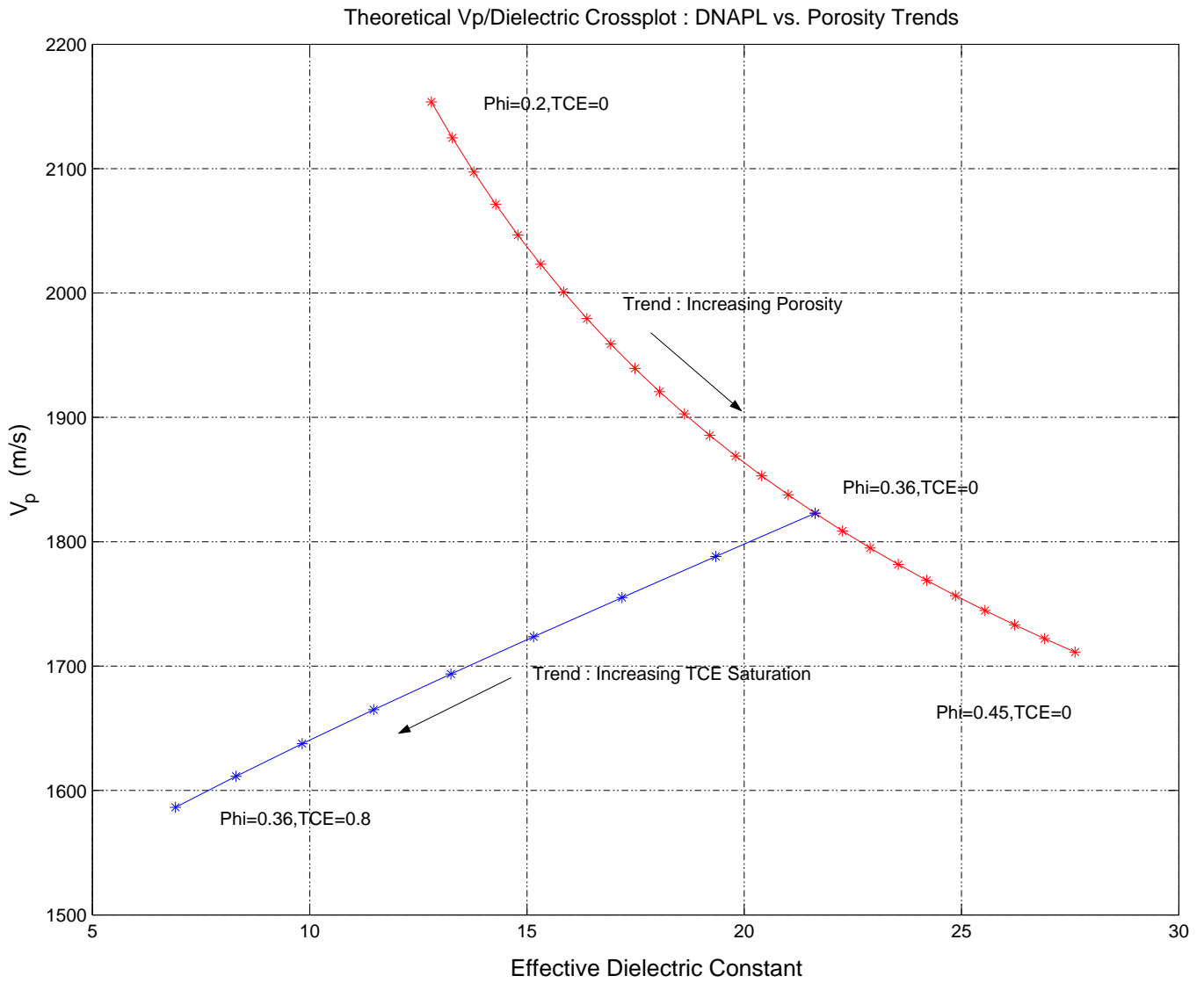


Figure 3: Theoretical V_p /dielectric constant cross-plot for a sand with either TCE saturation or porosity variations (ϕ = porosity)

2.2 Quantitative Integration of Tomography Results: Pitfalls

While cross-plots like Figure [3] are commonly generated from laboratory core measurements or high quality logging data, they are seldom used for analyzing tomography results due to a host of inconsistencies in the integration step. Ultimately, we would like to apply appropriately upscaled petrophysical relationships to a set of tomographic images with different data sources (dielectric constant, P and S-wave velocity etc.) and derive either secondary properties such as fluid saturation characteristics or more heuristic attributes which might provide a useful proxy indicator for NAPLs.

One of the most significant barriers to the quantitative use of even individual tomographic images is the presence of artifacts in the final inversion result, possibly caused by aperture limitation, irregular survey coverage, errors in picking, positioning, or discretization, and even fundamental physical inconsistencies between the way wave propagation actually occurs and the modeling scheme embedded in the tomography algorithm. At the integration step we are also forced to consider inevitable questions of scale; seldom are the resolving powers of two different geophysical measurements identical. This implies that even after inversion, seismic and radar images have different spatial averaging properties.

2.3 Preprocessing

After data collection we performed two stages of preprocessing. The first stage involved very standard operations, specifically file format conversion, the addition of trace geometry information, the manual removal of very low S/N traces, low cut filtering, and traveltimes picking. One of the largest differences observed between the radar and seismic datasets was the mismatch of angular apertures; while high angle rays in the seismic profiles could often be picked, the radar profiles were typically limited to an angular aperture of approximately ± 45 degrees from the horizontal due to the radiation pattern of the source and receiver antennas. The second stage of preprocessing aimed to make the data footprints of the seismic and radar surveys more similar in order to reduce artifacts when the separately processed tomograms were combined. The angular aperture of the seismic data was truncated on a source-by-source basis to conform with maximum aperture present in the radar dataset. In regions where both seismic and radar picks were available, we had sufficient spatial sampling to interpolate both datasets onto the same source/receiver position grid to exactly match portions of the survey geometry. In zones where source gathers from one of the two datasets were not pickable at low angle, no matching step outside of ± 45 degree aperture reduction was applied. This resulted in some coverage inconsistencies, particularly in the high seismic attenuation zones visible in Figure [2].

2.4 Traveltime Tomography Techniques

Our goal in designing the second tomographic processing flow was to choose an algorithm which could consistently recover from poor data coverage in the high attenuation zone, provide images relatively free of ray-based artifacts, and would require a minimal number of user controlled “tuning” parameters which could bias the tomography results. While we are ultimately moving towards approaches which truly honor the physical resolving power of band-limited data by incorporating fresnel regions [20] [14], our current implementation only accomplishes this indirectly through use of convolutional quelling [19].

All ray-tracing was performed using straight rays, a reasonable assumption given the small (generally $< 10\%$) velocity contrasts present within the primary imaging zone. One region where significant GPR ray-bending occurred was within the vicinity of the capillary fringe. However, since the vadose transition region was not one of our imaging targets, the few rays which crossed this zone were discarded.

The tomographic imaging technique we decided to use is a two-step process which first generates a 1D model and then uses this layered image as a prior for a 2D inversion, similar to the technique described in [35]. The 1D problem is usually very well resolved. Even in regions where significant gaps in data coverage exist, there are usually enough rays passing through a given layer to allow a velocity estimate, although the variance of the resulting estimate may be high. The layered inversion is parametrized as a stack of equal height, constant slowness sections. Regularization constraints are added with a one-dimensional 1st derivative operator which favors flat models. The generalized inverse for the resulting system, with the addition of the regularization term is

$$G_1^{-g} = [G_1^T G_1 + \lambda_1^2 (W_{m1}^T W_{m1})]^{-1} G_1^T \quad (1)$$

where G_1 is the kernel for the layered inversion problem, λ_1 is a regularization parameter, and W_{m1} is the 1st derivative model weighting matrix. W_{m1} uses forward differences with appropriate treatment of boundary points. The resulting 1D model estimate can then be written in terms of the generalized inverse as

$$m_{1_{est}} = G_1^{-g} d. \quad (2)$$

Since the layered model has only a small number of parameters, the generalized inverse is calculated using the singular value decomposition (SVD).

The Generalized Cross-Validation technique (GCV) [12] [33] is used to determine an appropriate regularization parameter for the 1D problem without having to assume a-priori a particular noise level. The GCV technique attempts to choose a regularization parameter resulting in a “robust” solution, i.e. a λ value which allows reliable prediction of the model if any single data point is discarded. $GVCV(\lambda)$, the metric which the GCV technique uses to judge the fitness of a particular choice of regularization or parametrization is

$$GVCV(\lambda) = \frac{\|(I - H_1) d\|^2}{Trace(I - H_1)^2} \quad (3)$$

where H_1 , the data resolution matrix, implicitly contains λ_1 since $H_1 = G_1 G_1^{-g}$. The GCV criterion is minimized over the space of reasonable regularization parameters. This is a 1D minimization problem requiring calculation of G_1^{-g} and H for a large number of λ_1 values. The λ_1 value that minimizes equation [3] is then used to evaluate the 1D tomography solution [2]. One common problem with the GCV approach is that GCV metric (3) often has a wide shallow minimum resulting in uncertainty as to the appropriate λ [15] although we did not have this difficulty in our 1D inversions.

The 2D tomography problem is parametrized as a rectilinear mesh of constant slowness pixels and is solved using $m_{1_{est}}$ as a prior. In reality, $m_{1_{est}}$ is not really prior information since it is derived from the same data used to estimate $m_{2_{est}}$. However, including a layered prior for the 2D problem generates a solution which effectively “defaults” to a 1D model in regions where the 2D solution is

poorly resolved. If we let G_2 be the kernel for the 2D tomography problem, the solution with our 1D prior and a natural generalized inverse would be

$$m_{2_{est}} = m_{1_{est}} + G_2^{-g}[d - G_2 m_{1_{est}}]. \quad (4)$$

A bit of algebraic manipulation and use of the definition of the model resolution matrix, $R = G^{-g}G$, yields the alternative form,

$$m_{2_{est}} = G_2^{-g} d + (I - R_2) m_{1_{est}} \quad (5)$$

which shows that information from the 1D solution is only used in cases where the 2D solution lacks sufficient resolution. If the 2D model is perfectly resolved ($R_2 = I$), the resulting tomogram does not include any information from the layered estimate. Since computation of R_2 is expensive, equation [4] is solved unless the model resolution matrix is desired for more complete analysis of the solution. To maintain dimensional consistency, the layered prior used in the 2D problem is resampled onto the 2D grid; typically the same depth spacing is used for both inversions so no interpolation step is required. The end result of the 1D/2D tomography process are images which provide reasonable 1D velocity estimates in regions with poor ray coverage without sacrificing lateral resolution in other sections of the profile.

While the kernel for the 2D problem, G_2 , is initially computed using infinitesimal rays, these rays are broadened using the convolutional quelling technique [19] [26] to heuristically account for the effects of band-limitation in both our radar and seismic experiments. The maximum width of the quelling filter is chosen to be a $\frac{1}{2}$ wavelength, where a single wavelength value derived from the mean velocity of the 1D model and the median centroid frequency of all incorporated traces is used for the entire kernel. The resulting fat rays limit the resolution of the final image to levels consistent with the recorded signal bandwidth. However, these broadened rays are not the ideal approximation to fresnel zones since they lack variations in width along the length of the ray and the appropriate off-axis weighting properties. In this paper we do not explicitly show the kernel and model reweighting steps from the convolutional quelling technique in our derivations. Reference [19] provides complete details on the implementation of convolutional quelling in a least-squares context.

The natural generalized inverse (G_2^{-g}) for the 2D problem (5) is computed using the truncated singular value decomposition (TSVD) [18]. If we write the SVD of G_2 as

$$G_2 = U_2 \Lambda_2 V_2^T \quad (6)$$

where U_2 and V_2 are the left and right eigenvectors and Λ is the diagonal eigenvalue matrix, then we can write the natural generalized inverse of G_2 as

$$G_2^{-g} = V_{2_p} \Lambda_{2_p}^{-1} U_{2_p}^T \quad (7)$$

where the p subscript denotes truncation at the p th eigenvalue. Initially, we attempted to use the GCV criterion to compute an appropriate cut-off point for the SVD truncation but irregularities in the GCV curve made this estimation difficult. The presence of correlated noise components in the traveltime pick data may be partially responsible for the failure of the GCV technique for the 2D inversion [15]. For larger problems, iterative techniques such as LSQR [23] [32] coupled with the L-Curve method of regularization parameter determination would be more appropriate than use of

the SVD + GCV flow due to the SVD’s asymptotic computational cost of $O(m n^2)$ for m data and n model parameters and the fact that computation of the GCV metric requires the data resolution matrix (H).

We typically calculate both the seismic and radar tomograms on matching rectilinear grids so that both dielectric constant and V_p values are available at the same spatial locations. However, this superposition of meshes does not mean that the averaging properties of the radar and seismic kernel are identical since the quelling widths and regularization parameters for each dataset are determined independently.

2.5 Post-Processing and Rock Physics Integration

With radar and seismic tomograms calculated for the same profile, the final integration of the two datasets for NAPL detection can take several forms. In the simplest case where only qualitative interpretation is performed on the two datasets, we line up our tomograms with any axillary information including core descriptions, well logs, and water sampling data and look for regions within the saturated zone with low dielectric constant values, low seismic velocities, and no consistent lithological explanation. To interpret more subtle variations in properties, a quantitative approach based on rock physics would be desirable. Ideally, an inverse petrophysical model which consistently describes both the dielectric and acoustic properties of sediments partially saturated with NAPLs could be used to combine the two tomograms to yield a map of porosity and NAPL saturation. In practice this is generally not feasible due to the physical complexity of unconsolidated sediments, the presence of variations in clay content, and a variety of scaling errors in both petrophysical relationships and the imaging process. A slightly less ambitious approach might involve the use of property cross-plots generated from tomographic images to identify trends associated with NAPL saturation. Although the cross-plot trends might not be equivalent to those generated from theoretical or core-scale experimental models, general features could provide guidance in the qualitative separation of lithology from saturation effects. Although we have generated V_p /dielectric cross-plots for several well pairs, we are currently carrying out laboratory calibration measurements to better understand the observed property trends.

3 Two Integrated Seismic/Radar Crosswell Profiles

We now apply the processing approach described in Section 2 to two crosswell profiles at the Pinellas NE site, one within the NAPL contaminated region (Figure [4], ROI 1, G14-G15) and one within a cleaner portion of the site (Figure [5] ROI 2 : G19-G20). Both Figures show local CPT lithology estimates and natural gamma logs in addition to crosswell radar and seismic tomograms. Figure [6] shows the tomograms plotted with the same color scale for property comparisons between the two well pairs. Figures [5] and [4] use different linear colorscales to enhance smaller anomalies. Due to the high seismic attenuation and consequently poor ray coverage, the region between -1 and -3 m elevation in the G14-G15 seismic profile (Figure [4]) only includes 1D model variations; this is a result of our hybrid 1D/2D formulation (see equations [4] [5]) . This region, labeled (Z1) in Figures [4] and [6], also has the largest velocity uncertainty since the weak high angle rays which pass through this zone are the most difficult to pick.

The top of the Lower Surficial Aquifer was consistently located in the crosswell radar tomograms and matched the CPT derived textural transition to within 20 cm. The radar surveys also detected

a subtle textural transition at an elevation of -0.25 m, a region with a gradual increase in fine particle components which is also visible on the gamma logs. The observed transitions in radar velocity can be largely explained by changes in volumetric water content due to variations in porosity/sorting, or in the case of the lower aquifer boundary, water trapped within the clay component. More striking than the features visible within the crosswell radar images is the lack of a high radar velocity region near the Hawthorn formation or the Lower Surficial Aquifer boundary in the G14-G15 profile, which we expected to be the best signature of a zone of high NAPL saturation. In fact, the absolute radar velocities were higher for the lower surficial aquifer in the G19-G20 profile, suggesting that the NAPL saturations in the ROI 1 contaminated region are low, if present.

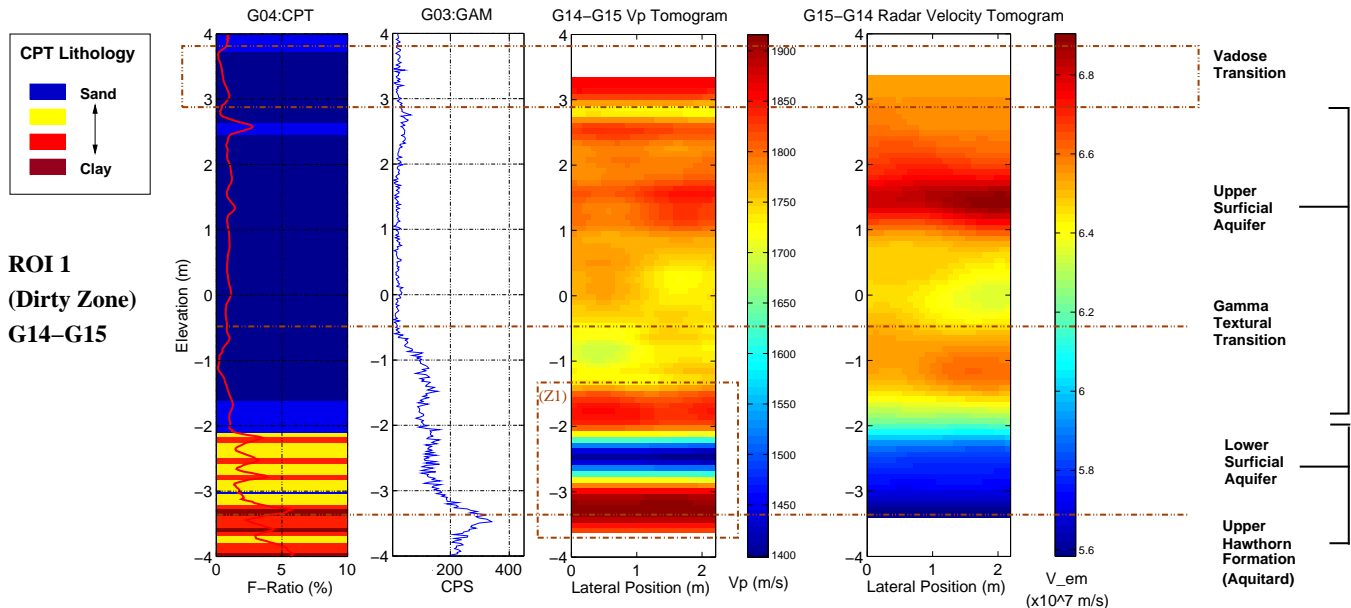


Figure 4: ROI 1 : G14-G15 : Dirty Well Pair

3.1 Working towards Quantitative Integration

Despite questions of scale and resolution consistency between the seismic and radar tomograms, we have started to examine V_p /dielectric crossplots generated from the Pinellas tomograms to help understand the trends associated with natural lithological transitions. Figure [7] depicts the V_p /dielectric crossplot for every point in both the G19-G20 and the G14-G15 profiles. The internal structure of the crossplot is dominated by vertical property variations with smaller lateral variations generating the internal “loops” in both curves. The region in Figure [7] labeled (Z1) corresponds to cross-plot points within the poorly resolved lower region of the G14-G15 seismic profile and should be treated with some caution. We have not yet made the core-scale calibration measurements required to interpret Figure [7] with confidence but we are currently in the process of building a dual dielectric/acoustic property model based on samples extracted from several locations at the Pinellas NE site. Using ultrasonic pulse transmission techniques and time domain reflectometry (TDR) we hope to both unravel some of the cross-plot’s structure and make some more quantitative statements concerning the sensitivity of radar measurements to NAPL saturation within the different lithologies present at Pinellas.

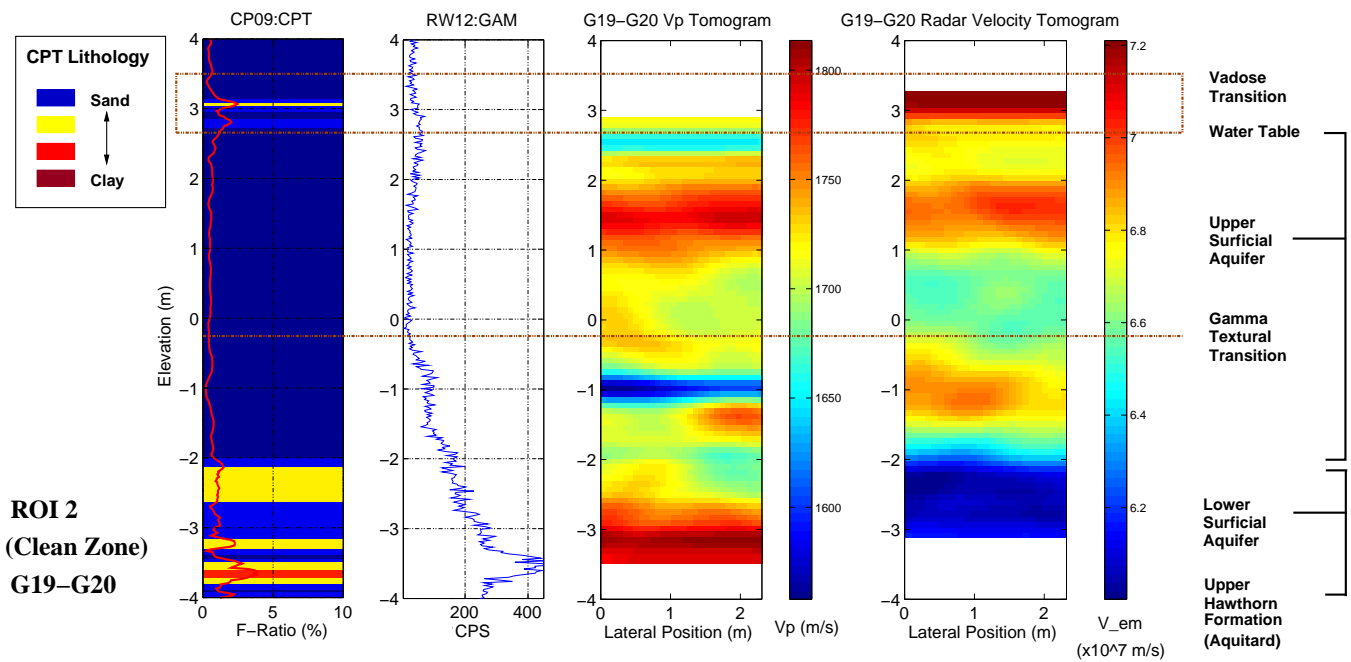


Figure 5: ROI 2 : G19-G20 : Clean Well Pair

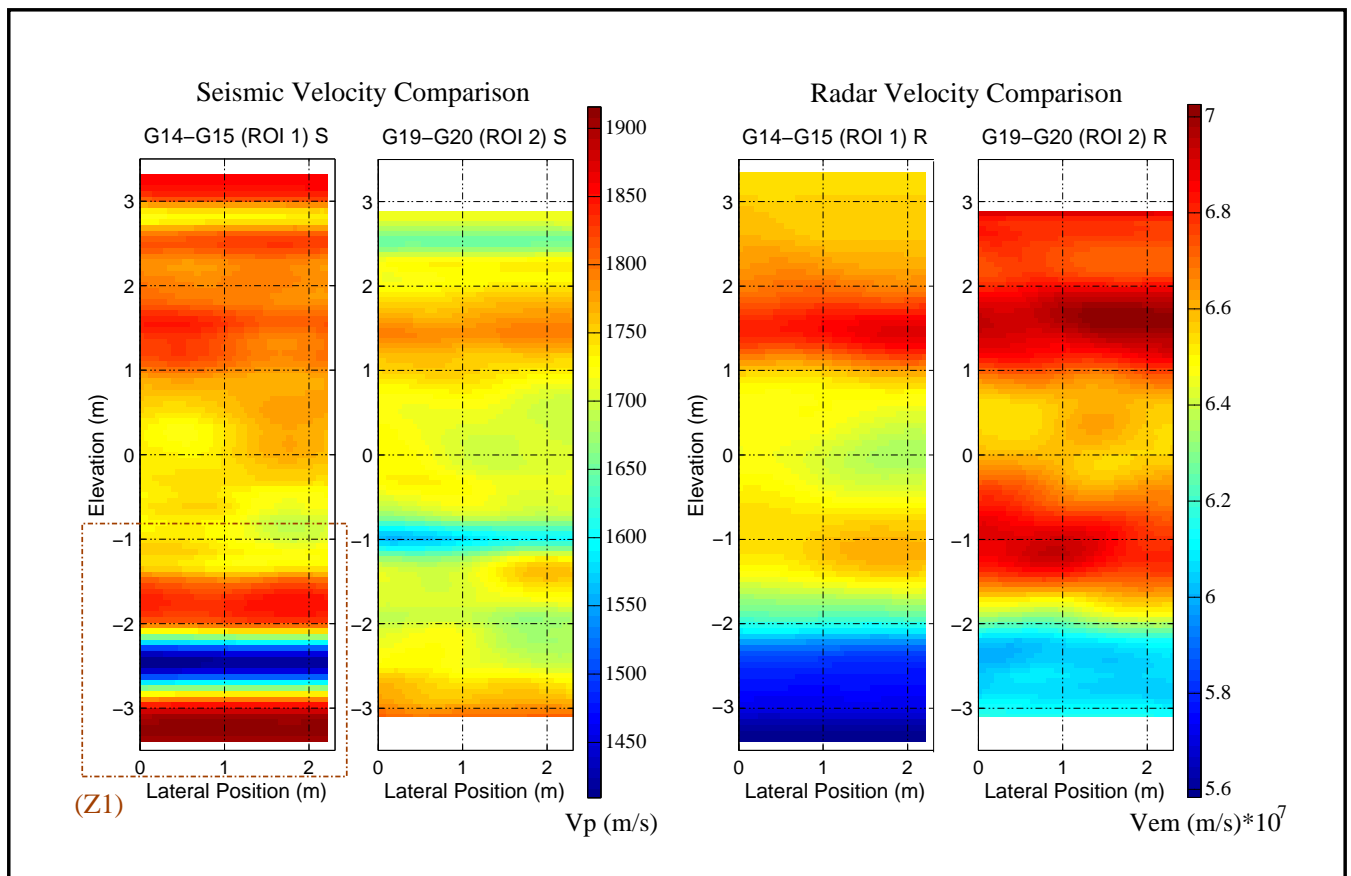


Figure 6: ROI 1 + ROI 2 Tomographic Comparison : Same Color Scale

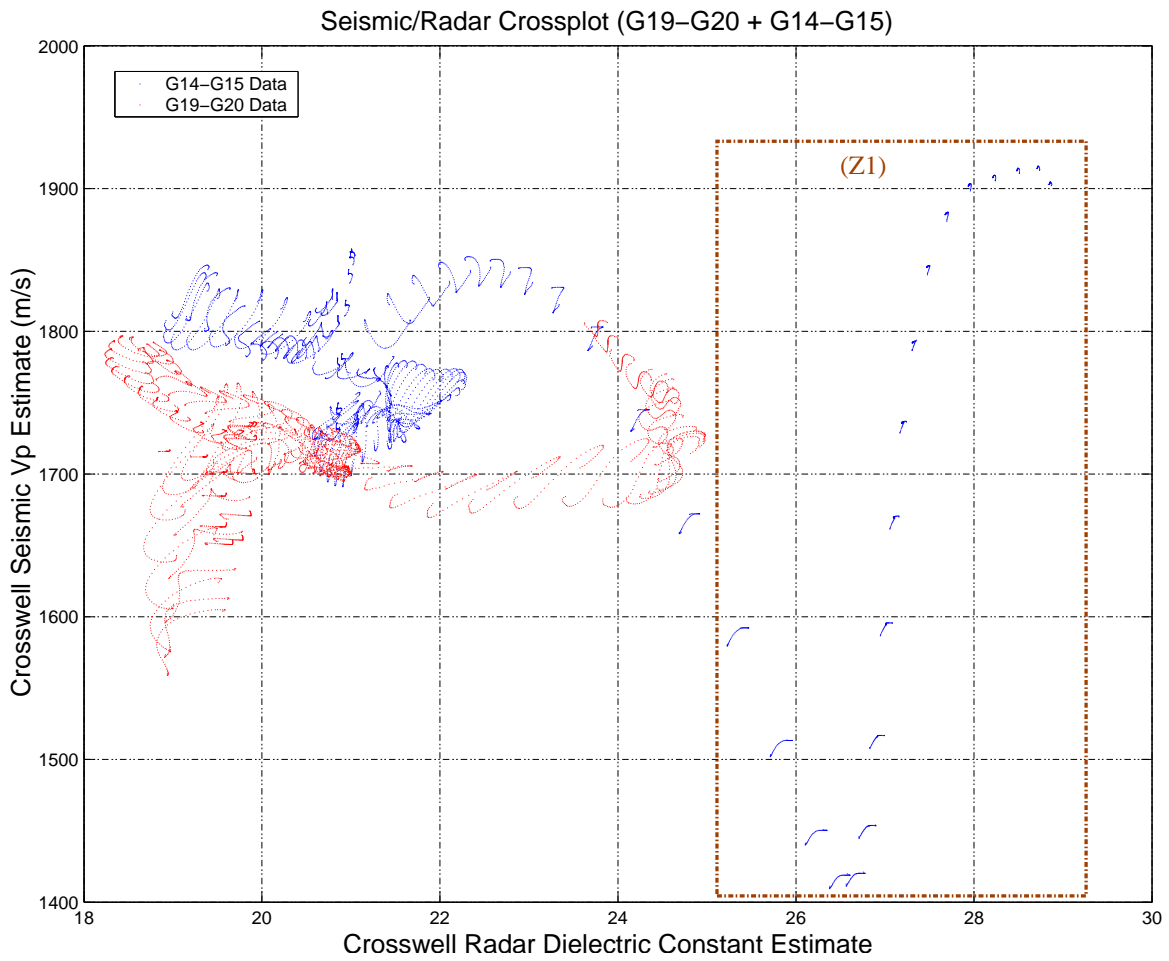


Figure 7: Experimental seismic/radar crossplot for the G19-G20 and G14-G15 well pairs derived from crosswell tomography measurements

Another problem with the integration of crosswell seismic and radar measurements at Pinellas is the large difference in resolution between the two measurement techniques. We calculated maps of the local wavelength of both the seismic and radar profiles for the G19-G20 well pair (Figure [8]) using the velocity tomograms and the mean centroid frequency of each survey. The third panel in Figure [8] shows the point-by-point ratio of local seismic wavelength to local radar wavelength, which ranges between 0.42 and 0.55 for the G19-G20 surveys. To truly integrate the seismic and radar images we must eventually address the different averaging patterns of the two property estimates by either a wave-consistent upscaling or statistical downscaling approach.

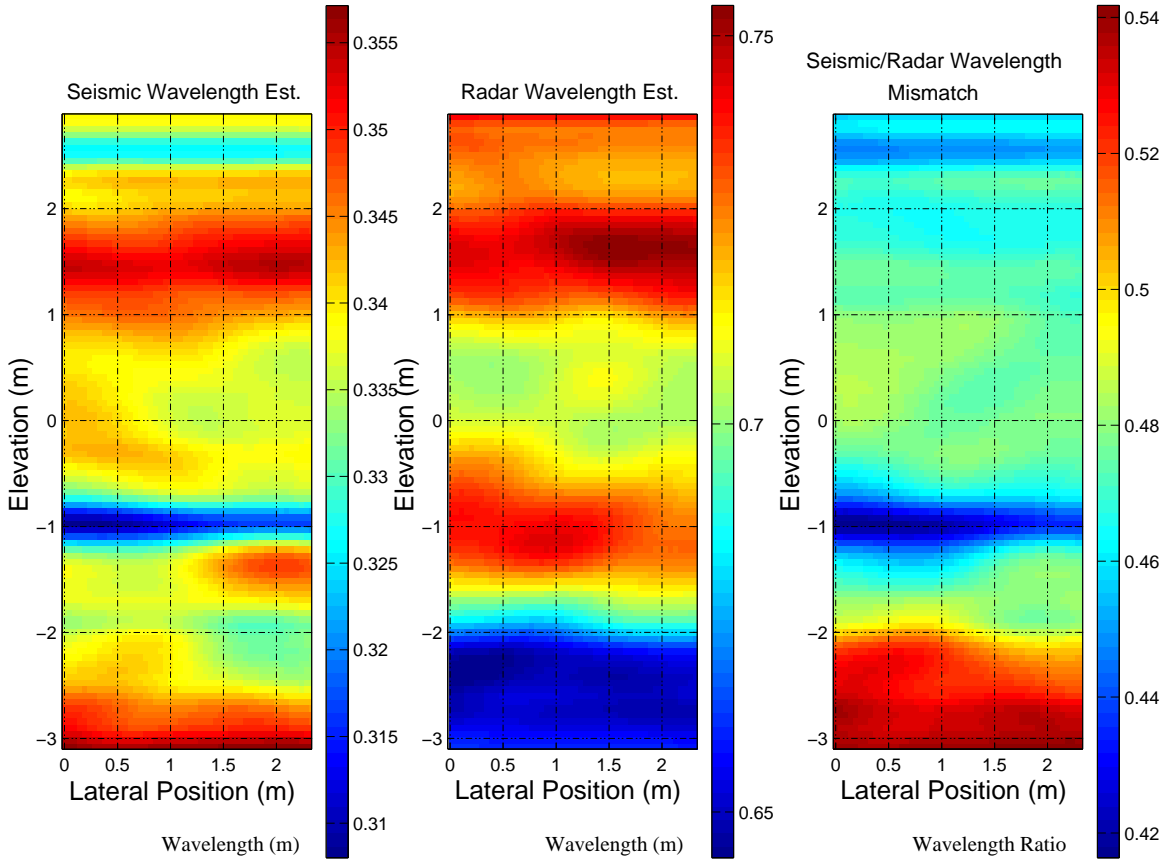


Figure 8: Local estimates of wavelength and wavelength mismatch for the G19-G20 seismic and radar tomograms

4 Understanding the Attenuating Region: A Gas Mechanism?

A dominant feature in the crosswell seismic datasets collected at Pinellas was the presence of a highly attenuating region centered around an absolute elevation of approximately -2 m. Figure [9] shows a comparison of the zero-offset seismic sections for the G19-G20 well pair (ROI 2) and the G14-G15 well pair (ROI 1). Label (a) indicates the depth section characterized by very low signal strength, straddling the boundary between the upper and lower surficial aquifers. The zone of attenuation

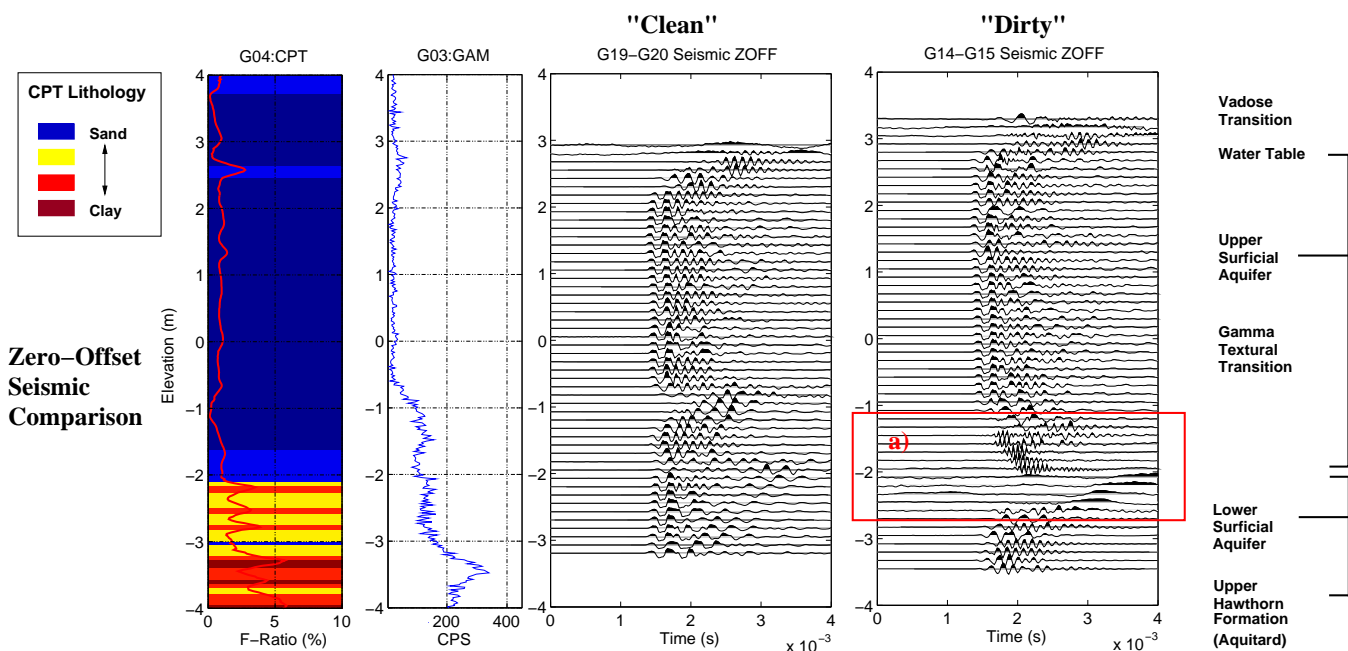


Figure 9: Comparison of the zero offset sections for the G19-G20 and G14-G15 crosswell seismic profiles

laterally coincides with the region of the site where high levels of aqueous phase contaminant were measured and some direct NAPL samples taken. No corresponding region of unusual dielectric behavior was noted in this region. When the low signal region was initially observed, we considered several possibilities besides attenuation within the media. A shift in borehole coupling properties was ruled out by examination of source and receiver gathers within the attenuating region. All of the wells within the ROI 1 and ROI 2 pairs were drilled using rotary sonic and cased with 4 in. PVC pipe. Since velocity contrasts within the crosswell profiles are relatively small, geometric shadow zones also seem unlikely. Quantitative estimation of attenuation within the low signal zone is a difficult task since few rays with sufficient energy to pick cross the zone.

Lithological, fluid, and gas effects were all initial candidates for the attenuation mechanism but a purely lithological explanation seemed the least likely due to the lack of any large lateral textural trends in our section of the NE site. However, until further measurements are made, we cannot rule out lithology as a possible source. Several recent lab-scale investigations have considered seismic attenuation and velocity changes due to the presence of NAPLs [11] [30]. These studies demonstrated that P-wave attenuation is considerably more sensitive to NAPL saturation than P-wave velocity for lab-scale core measurements. A direct NAPL-patch scattering mechanism might be a possible source for the attenuating zone. However, using the previously discussed CRIM model as a simple guide, we would expect bulk TCE saturations over 20% to be visible as an anomalously fast region on the radar tomograms. Additionally, the attenuation mechanism functioning in ultrasonic NAPL experiments (100-200 khz) may not be operative at field crosswell frequencies (1-8 khz). A gas-related mechanism seems to be the most plausible scenario, since small volumetric gas contents can significantly affect seismic wave propagation without a large corresponding radar signature. On a more detailed level, we can imagine scattering off of gassy patches, a patch equilibration mechanism [8], or direct attenuation related to bubble resonance

[2] [3] [34]. However, any conclusive determination of the operative attenuation mechanism would require either another detailed coring effort with gas and fluid sampling or possibly a secondary suite of high-resolution crosswell shear wave measurements to constrain the saturation models.

If we assume that a gas mechanism is the primary source of attenuation, several possible gas sources could be posited. The high levels of vinyl chloride (VC), a product of the reductive dechlorination of TCE or DCE, found in wells M17D and RW06 suggest that contaminant degradation driven by biogenic activity might be a possible gas source. If this pathway were conclusively proven, gas-generated seismic attenuation might be useful as a proxy indicator for the presence of NAPLs at Pinellas. Non-condensable gas generated by the auger steam-stripping treatment might also be responsible, although attenuation levels do not seem to be well correlated with proximity to the augered zones. Pressure reduction, due to groundwater withdrawal for plume containment, and the resultant degassing might also be responsible for the attenuating zone.

5 Conclusion and Future Work

Although our preliminary work at the Pinellas NE site has not yet yielded concrete geophysical evidence for the presence of NAPLs in the subsurface, we remain hopeful that ongoing improvements in our image reconstruction and data integration algorithms coupled with a better understanding of site soil properties will allow a more conclusive answer to the remote NAPL detection problem. A detailed ground-truthing process based on careful coring and prompt chemical analysis of the extracted pore fluids would be the best way to test the efficacy of our geophysical analysis. Crosswell shear-wave measurements using locking three-component receivers might also provide us with a more detailed model of saturation-driven seismic anomalies in the near-surface, especially within the problematic zone of high attenuation.

Acknowledgments

This work was funded by the Subsurface Contamination Focus Area of the Environmental Management Program of the USDOE, under contract # DE-AC-03-76F0098. We would also like to thank the EPA for funding the first author through the STAR Fellowship program and the Stanford Department of Geophysics for funding through the Chair's Fellowship for Intergroup Research. This research would not have been possible without the cooperation of the DOE Pinellas Site Staff including Dave Ingle and the S.M. Stoller Corp. Crew. We would also like to thank Cecil Hoffpauier (LBNL), Philip Rizzo (LBNL), and Jaime Urban (Stanford) for assistance in the collection of field data at Pinellas.

References

- [1] S.F. Al-Azzawi, A.M. Awwad, A.H. Al-Dujaili, and M.K. Al-Noori. Dielectric constants and excess volumes of 2-Pyrrolidone + Water at several temperatures. *Journal Of Chemical Engineering Data*, 35:463–466, 1990. 5
- [2] A.L. Anderson and L.D. Hampton. Acoustics of gas-bearing sediments I. Background. *Journal of the Acoustical Society of America*, 67(6):1865–1889, June 1980. 16

- [3] A.L. Anderson and L.D. Hampton. Acoustics of gas-bearing sediments II. Measurements and models. *Journal of the Acoustical Society of America*, 67(6):1890–1903, June 1980. 16
- [4] R. Bachrach and A. Nur. Same wavelength GPR and ultra shallow seismic reflection on a river point bar: Sand stratigraphy and water table complexity. *Expanded Abstract, Society Of Exploration Geophysics Annual Meeting, 1998*, 1:840–844, 1998. 5
- [5] G.S. Baker, R. Plumb, D.W. Steeples, M. Pavlovic and C. Schmeissner. Coincident GPR and ultra-shallow seismic imaging in the Arkansas River Valley, Great Bend, Kansas. *Expanded Abstract, Society Of Exploration Geophysics Annual Meeting, 1998*, 1:859–861, 1998. 5
- [6] M.L. Brewster and A.P. Annan. Ground-penetrating radar monitoring of a controlled dnapl release: 200 mhz radar. *Geophysics*, 59(8):1211–1221, 1994. 1, 5
- [7] M.L. Brewster, A.P. Annan, J.P. Greenhouse, B̃.H. Kueper, G.R. Olhoeft, J.D. Redman, and K̃.A. Sander. Observed migration of a controlled DNAPL release by geophysical methods. *Ground Water*, 33(6):977–987. 1, 5
- [8] N.C. Dutta and H. Ode. Attenuation and dispersion of compressional waves in fluid-filled porous rocks with partial gas saturation (white model) - part I: Biot theory, part II: Results. *Geophysics*, 44:1777–1805, 1979. 15
- [9] F. Gassmann. Uber die elastizitat poroser medien. *Vier. der Natur. Gessellschaft in Zurich*, 96:1–23, 1951. 5
- [10] J.T. Geller, M.B. Kowalsky, P.K. Seifert, and K̃.T. Nihei. Acoustic detection of immiscible liquids in sand. *Geophysical Research Letters*, 27(3):417–420, 2000. 2, 5
- [11] J.T. Geller and L.R. Myer. Ultrasonic imaging of organic liquid contaminants in unconsolidated porous media. *Contaminant Hydrology*, 19:85–104, 1995. 2, 5, 15
- [12] G.H. Golub, M.T. Heath, and G. Wahba. Generalized cross-validation as a method for choosing a good ridge parameter. *Technometrics*, 21:215–223, 1979. 8
- [13] T.W. Griffin and K.W. Watson. A comparison of field techniques for confirming dense nonaqueous phase liquids. *Ground Water Monitoring and Remediation*, 22(2):48–59, 2002. 1
- [14] G.Schuster and A. Quintus-Bosz. Wavepath eikonal travelttime inversion: Theory. *Geophysics*, 58:1314–1323, 1993. 7
- [15] P.C. Hansen. Analysis of discrete ill-posed problems by means of the L-curve. *SIAM Review*, 34(4):561–580. 8, 9
- [16] M.B. Kowalsky, J.T. Geller, P.K. Seifert, K̃.T. Nihei, and L.R. Myer. Acoustic visibility of immiscible liquids in poorly consolidated sand. *Expanded Abstract, Society Of Exploration Geophysics Annual Meeting, 1998*, page 4, 1998. 2
- [17] G. Mavko, T. Mukerji, and J. Dvorkin. *The Rock Physics Handbook: Tools For Seismic Analysis In Porous Media*. Cambridge University Press, 1998. 5
- [18] W. Menke. *Geophysical Data Analysis : Discrete Inverse Theory*. Academic Press, 1984. 9

- [19] K.A. Meyerholtz, G.L. Pavlis, and S.S. Szpakowski. Convolutional quelling in seismic tomography. *Geophysics*, 54(5):570–580. 7, 9
- [20] R. Michelena and J. Harris. Tomographic travelttime inversion using natural pixels. *Geophysics*, 56:635–644, 1991. 7
- [21] R.D. Mindlin. Compliance of elastic bodies in contact. *Journal Of Applied Mechanics*, 16:259,268, 1949. 5
- [22] J. Nath. Ultrasonic velocities, relative permittivities, and refractive indices for binary liquid mixtures of Trichloroethylene with Pyridine amd Quinoline. *Fluid Phase Equilibria*, 109:39–51, 1995. 5
- [23] C.C. Paige and M.A. Saunders. LSQR: An algorithm for sparse linear equations and sparse least squares. *Trans. Math. Softw.*, 8:43–71, 1982. 9
- [24] J.E. Peterson. *The Application of Algebraic Reconstruction Techniques to Geophysical Problems*. PhD thesis, 1986. 4
- [25] J.E. Peterson. Pre-inversion corrections and analysis of radar tomographic data. *Journal Of Environmental And Engineering Geophysics*, 6:1–18, March 2001. 4
- [26] W.S. Phillips and M.C. Fehler. Traveltime tomography : A comparison of popular methods. *Geophysics*, 56(10):1639–1649, 1991. 9
- [27] J.D. Redman. Geophysics and the solvents-in-groundwater program. *Symposium on the Application of Geophysics to Engineering and Environmental Engineering, Soc. Eng. Min. Expl. Geophys.*, pages 375–382, 1992. 1, 5
- [28] A. Reuss. Berechnung der fließgrenzen von mischkristallen auf grund der plastizitatbedingung fur eikkristalle. *Zeitschrift fur Angewandte Mathematik und Mechanik*, (9):49–58, 1929. 5
- [29] K.A. Sander, G.R. Olhoeft, and J.E. Lucius. Surface and borehole radar monitoring of a DNAPL spill in 3d versus frequency, look angle, and time. *Symposium on the Application of Geophysics to Engineering and Environmental Engineering*, 2:455–469, 1992. 1, 5
- [30] P.K. Seifert, J.T. Geller, and L.R. Johnson. Effect of P-wave scattering on velocity and attenuation in unconsolidated sand saturated with immiscible liquids. *Geophysics*, 63(1):161–170, 1998. 2, 5, 15
- [31] T.J. Temples, M.G. Waddell, and W. Domoracki. Non-invasive determination of the location and distribution of dnapl using advanced seismic reflection techniques. *Groundwater*, 39(3):465–474, 2001. 1
- [32] A van der Sluis and H.A. van der Horst. Numerical solution of large, sparse linear algebraic systems arising from tomographic problems. In G. Nolet, editor, *Seismic Tomography With Applications in Global Seismology and Exploration Geophysics*, chapter 3. 1987. 9
- [33] G. Wahba. *Spline Models for Observational Data*, volume 59 of *CBMS-NSF Regional Conference Series in Applied Mathematics*. Society For Industrial And Applied Mathematics, 1990. 8
- [34] R.H. Wilkens and M.D. Richardson. The influence of gas bubbles on sediment acoustic properties : in situ, laboratory, and theoretical results from Eckernforde Bay, Baltic Sea. *Continental Shelf Research*, 18:1859–1892, 1998. 16

- [35] H.W. Zhou, J.A. McDonald, C.A. Link, and J. Jech. Constraining the magnitude of velocity perturbations in travelttime tomography. *Journal Of Seismic Exploration*, 2:365–380, 1993. 8